ResearchGate

See discussions, stats, and author profiles for this publication at: https://www.researchgate.net/publication/373251160

A platypus-inspired electro-mechanosensory finger for remote control and tactile sensing

Article *in* Nano Energy · August 2023

DOI: 10.1016/j.nanoen.2023.108790

CITATIONS
0

READS
128

13 authors, including:

Shilong Mu
Tsinghua University
7 PUBLICATIONS **5** CITATIONS
SEE PROFILE

Zihan Wang
Tsinghua University
26 PUBLICATIONS **411** CITATIONS
SEE PROFILE

Huaze Tang
Tsinghua University
12 PUBLICATIONS **14** CITATIONS
SEE PROFILE

All content following this page was uploaded by Zihan Wang on 02 October 2023.

The user has requested enhancement of the downloaded file.

Nano Energy 116 (2023) 108790

Contents lists available at ScienceDirect

Nano Energy

journal homepage: www.elsevier.com/locate/nanoen

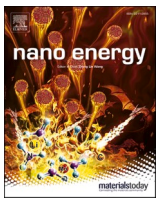

Full paper

A platypus-inspired electro-mechanosensory finger for remote control and tactile sensing

Shilong Mu [a,1], Shoujie Li [a,1], Hongfa Zhao [a,1], Zihan Wang [a], Xiao Xiao [b], Xiao Xiao [c,d,e], Zenan Lin [a], Ziwu Song [a], Huaze Tang [a], Qinghao Xu [a], Dongkai Wang [a], Wang Wei Lee [f,*], Changsheng Wu [d,e,g,**], Wenbo Ding [a,h,***]

[a] Tsinghua-Berkeley Shenzhen Institute, Shenzhen International Graduate School, Tsinghua University, Shenzhen 518055, China
[b] Shenzhen International Graduate School, Tsinghua University, Shenzhen 518055, China
[c] Department of Electrical and Computer Engineering, National University of Singapore, Singapore 117583, Singapore
[d] Institute for Health Innovation and Technology, National University of Singapore, Singapore 117599, Singapore
[e] SIA-NUS Digital Aviation Corporate Lab, National University of Singapore, Singapore 117602, Singapore
[f] Tencent Robotics X, Shenzhen 518054, China
[g] Department of Materials Science and Engineering, National University of Singapore, Singapore 117575, Singapore
[h] RISC-V International Open Source Laboratory, Shenzhen 518055, China

ARTICLE INFO

Keywords:
Bionic sensor
Triboelectric nanogenerator
Visuotactile sensor
Touchless sensing
Tactile sensing
Human-robot interaction

ABSTRACT

Advancement in human-robot interaction (HRI) is essential for the development of intelligent robots, but there lack paradigms to integrate remote control and tactile sensing for an ideal HRI. In this study, inspired by the platypus beak sense, we propose a bionic electro-mechanosensory finger (EM-Finger) synergizing triboelectric and visuotactile sensing for remote control and tactile perception. A triboelectric sensor array made of a patterned liquid-metal-polymer conductive (LMPC) layer encodes both touchless and tactile interactions with external objects into voltage signals in the air, and responds to electrical stimuli underwater for amphibious wireless communication. Besides, a three-dimensional finger-shaped visuotactile sensing system with the same LMPC layer as a reflector measures contact-induced deformation through marker detection and tracking methods. A bioinspired bimodal deep learning algorithm implements data fusion of triboelectric and visuotactile signals and achieves the classification of 18 common material types under varying contact forces with an accuracy of 94.4 %. The amphibious wireless communication capability of the triboelectric sensor array enables touchless HRI in the air and underwater, even in the presence of obstacles, while the whole system realizes high-resolution tactile sensing. By naturally integrating remote contorl and tactile sensing, the proposed EM-Finger could pave the way for enhanced HRI in machine intelligence.

1. Introduction

Advances in human-robot interaction (HRI) bring immense possibilities across diverse domains, such as virtual/augmented reality [1,2], healthcare [3], space exploration [4], and smart manufacturing [5]. As one of the most dominating yet challenging HRI methods, various tactile sensors have been designed based on different mechanical-to-electrical conversion mechanisms, such as piezoresistive [6,7], capacitive [8,9], magnetic [10,11], etc [12,13]. Meanwhile, visuotactile sensors using cameras to capture deformation-induced changes of contact surfaces, have emerged as an economical solution towards high-resolution tactile sensing [14–18]. However, most of existing tactile sensors cannot respond to non-contact stimuli, limiting the prior and accurate acquisition of object size [19], direction [20], and distance [21] during HRI. A paradigm to endow tactile sensors with touchless sensing capability is heavily desired for an ideal HRI that resembles the natural processes of

* Corresponding author.
** Corresponding author at: Institute for Health Innovation and Technology, National University of Singapore, Singapore 117599, Singapore.
*** Corresponding author at: Tsinghua-Berkeley Shenzhen Institute, Shenzhen International Graduate School, Tsinghua University, Shenzhen 518055, China.
E-mail addresses: wwlee@tencent.com (W.W. Lee), cwu@nus.edu.sg (C. Wu), ding.wenbo@sz.tsinghua.edu.cn (W. Ding).
[1] These authors contributed equally: Shilong Mu, Shoujie Li, Hongfa Zhao

https://doi.org/10.1016/j.nanoen.2023.108790
Received 6 August 2023; Received in revised form 13 August 2023; Accepted 14 August 2023
Available online 19 August 2023
2211-2855/© 2023 Elsevier Ltd. All rights reserved.

exploration and manipulation by organisms.

To this end, multisensory systems for both touchless and tactile perception have been developed with single or hybrid mechanisms. However, those with single mechanisms, e.g., triboelectric [22–24] or magnetic [25,26], are prone to suffer from decoupling touchless and tactile signals or interferences from external electric and magnetic fields, while those with hybrid ones, e.g., triboelectric and piezoresistive [27], optical and barometric [28], often possess limited tactile resolution or high cost in materials and fabrication. Moreover, previous reports typically have sensing units stacked on planar surfaces in a two-dimensional configuration, which can hardly realize omnidirectional perception in space [22,29–31]. In practice, to implement a compact, high-resolution, and omnidirectional multisensory system that supports both touchless and tactile sensing, remains a formidable challenge. Fortunately, inspiration from nature has led to the development of several smart electrosensory or mechanosensory systems [32–34]. Aquatic mammals [35,36], especially the platypus as shown in Fig. 1a, have evolved with sensory organs capable of detecting remote stimuli from bioelectrical signal and contact stimuli from mechanosensory signal [37–39]. Such fusion mechanisms have enabled platypus to hunt for prey from the mud in spite of dark waters.

Herein, inspired by the platypus beak sense, we propose a bionic electro-mechanosensory finger (EM-Finger) synergizing triboelectric and visuotactile sensing for remote control and tactile perception. Similar to how electrosensory nerve terminals help platypus gather electrical signal in murky water, the as-prepared triboelectric sensor array performs omnidirectional touchless sensing by leveraging the electrostatic induction effect and a three-dimensional (3D) finger-like structure. High-resolution multimodal tactile perception of contact pressure and surface texture is realized by a visuotactile sensor. The fusion of triboelectric and visuotactile signals leads to the identification of 18 material types under varying forces with an accuracy of 94.4 %, which is 67.4 % when only the triboelectric signal is available. Based on the designed EM-Finger, we implement an integrated HRI system capable of both touchless interaction and multimodal tactile sensing to perform remote control and object recognition in the air. The system also makes it possible for robots to conduct underwater tasks, including electrical stimuli-enabled wireless communication, tactile perception, object manipulation, and advances HRI in amphibious intelligent robots.

2. Results and discussion

2.1. Bimodal sensory design of EM-Finger

EM-Finger mimics platypus's multisensory system through the combination of a triboelectric sensor array and a finger-shaped visuotactile sensor. The beak of the platypus contains densely packed arrays of specialized receptor organs and their afferent nerves (Fig. 1b). These special receptor organs have electrosensory and mechanosensory functions. Specifically, the electroreceptors distributed in the soft dermal layer can detect the weak bioelectrical signals related to the muscle contraction of the prey, and mechanoreceptors can respond to contact

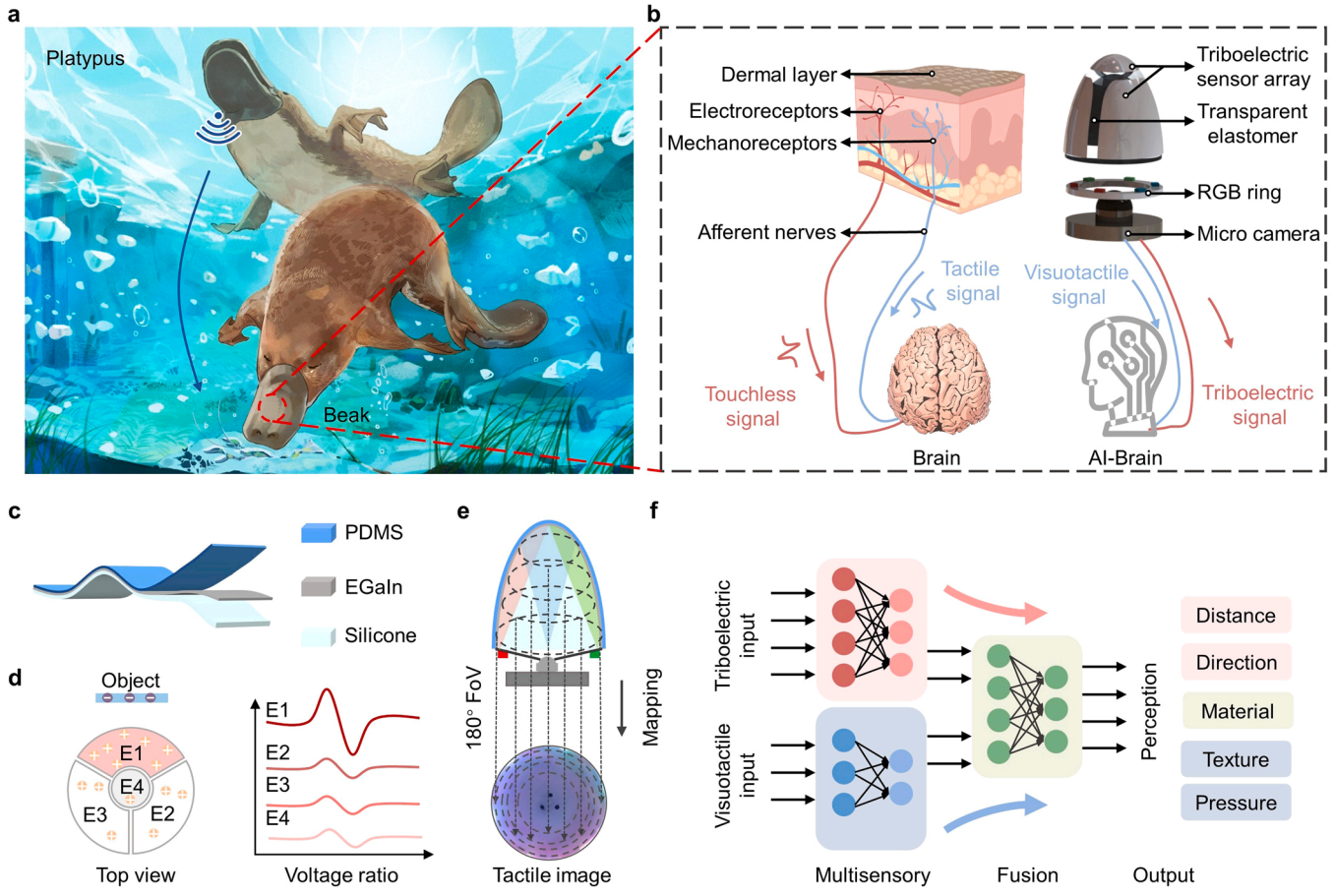

Fig. 1. Bioinspired bimodal sensory system. (a) Schematic diagram of a platypus feeding on underwater prey by receptors distributed in its beak. (b) The structure of (i) the platypus's bimodal sensory system and (ii) the bionic electro-mechanosensory finger (EM-Finger). (c) Structure of the soft triboelectric sensor distributed on the finger surface. (d) The touchless spatial sensing strategies and the top view of the finger. E1 to E4 represents the electrodes in the triboelectric sensor array. (e) Three-dimensional internal lighting structures are mapped to the tactile image. The internal lighting uses a LED ring. The internal image has three markers and is seen by a camera with a wild 180-degree field of view (FOV). (f) The data processing framework, which can process triboelectric and visuotactile signals separately and then fuse the data to realize the touchless and tactile sensory.

stimuli. Touchless and tactile stimuli lead to an increase in receptor cell membrane potential, which is then transmitted as impulse signals along the afferent nerves to the brain. Therefore, platypus dives with their eyes, ears and nose closed most of the time, they probably rely almost entirely on electrosensory and mechanosensory functions to locate prey and hunt from the mud.

Herein, the triboelectric sensor array can imitate the electroreceptors of the platypus beak to detect electrical stimuli based on electrostatic induction. Meanwhile, the visuotactile sensor extracts information from contact-induced deformation, corresponding to the numerous mechanoreceptors of platypus beak. The triboelectric sensor array is fabricated by spraying liquid-metal-polymer conductive (LMPC) ink through a mask on a finger-shaped transparent elastomer to form an electrode array (Fig. 1c). Then the conductive layer is encapsulated by a polydimethylsiloxane (PDMS) dielectric layer to prevent exfoliation and oxidation. Here, the LMPC layer simultaneously serves as the electrodes of the triboelectric sensor array and the reflector of the visuotactile sensor. As illustrated in Fig. 1d, the charge distribution on the electrode surface of the triboelectric sensor array is altered by electrostatic induction. This alteration encodes the object movement into multi-

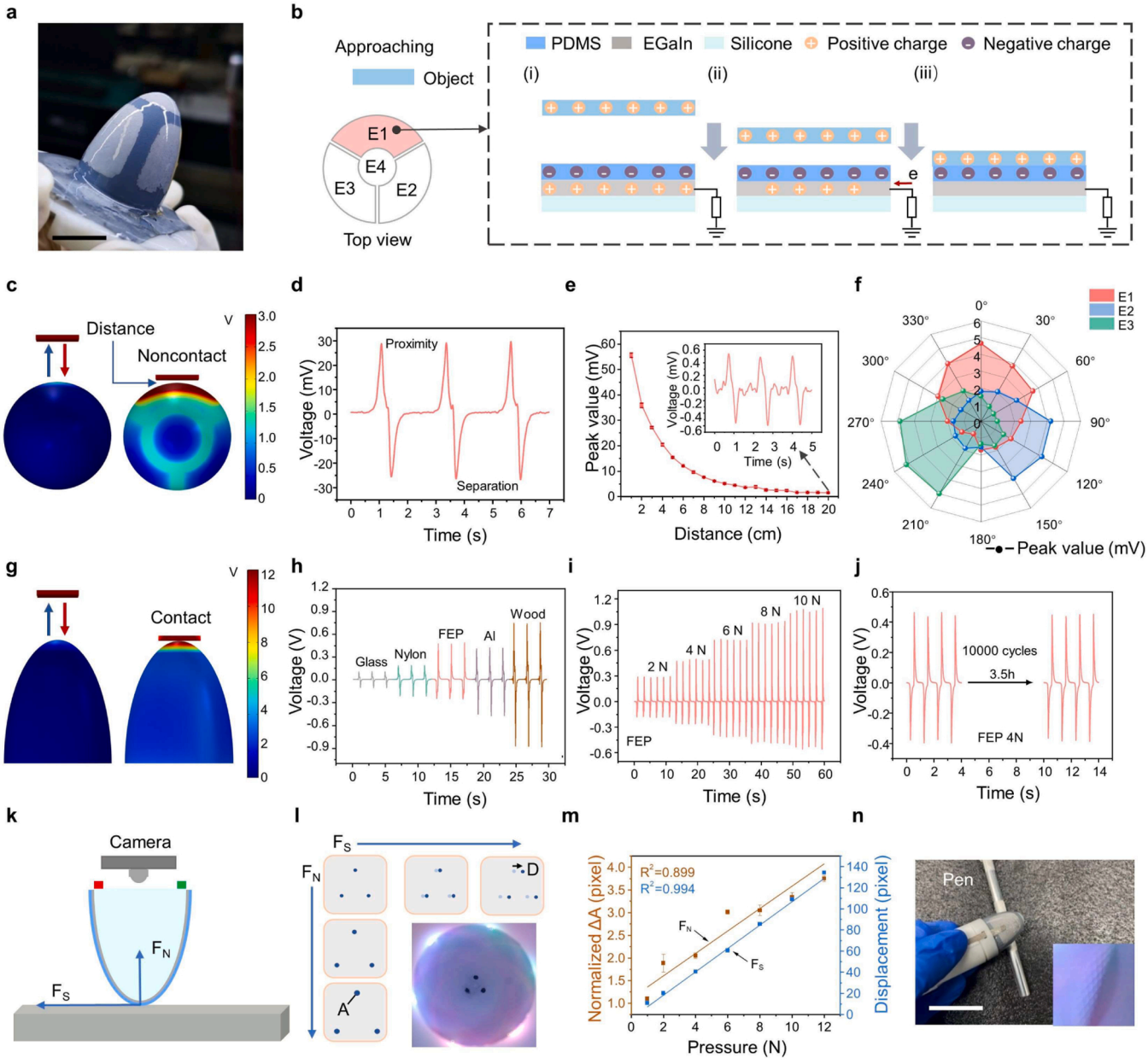

Fig. 2. Working mechanism and characterization of the EM-Finger. (a) Photograph of the EM-Finger prototype showing its triboelectric sensor array (scale bar: 1 cm). (b) The working mechanism of the triboelectric sensor. (c) Finite element analysis results of the potential distribution mechanism as the triboelectric layer approaches the E1 electrode on the EM-Finger side. The relationship between the motion pattern of the object and the corresponding voltage signal: (d) proximity-separation motion, (e) variable approach distance, and (f) spatial perceptibility. (g) Simulation of the potential change when the triboelectric layer contacts the E4 electrode on the fingertip of the EM-Finger. (h) Voltage waveforms output when the sensor identifies glass, nylon, FEP, Al, and wood. (i) Voltage waveforms are output by the sensor when contacting FEP at different pressures. (j) Sensing cycle performance of triboelectric sensor at 10,000 cycles, 3.5 h. (k) Schematic illustration of tactile sensing using a tactile image in the presence of normal and shear forces (F_N, F_S). (l) The principle of pressure sensing by the markers in the tactile image, where D denotes the moved distance and A denotes the normalized changed area. (m) Relationship between the normalized changed area and displacement of markers and the force generated by different directions. (n) Photograph of pressing EM-Finger on a pen with a pattern and the corresponding surface texture details (scale bar: 3 cm).

channel voltage pulses. Wherein, the electrodes in the triboelectric sensor array are marked as E1 to E4. The elastomer is mounted on a ring with a circular arrangement of red, green, and blue light-emitting diodes (RGB LEDs) (Fig. 1e). The application of RGB lighting can increase the contrast of images captured by a micro camera, which enables reflects more fine-grained deformation of the elastomer[40]. The varying force during contact is measured and recorded by tracking the movement of the markers on the transparent elastomer tip. Detailed illustrations of the mechanical structure and fabrication processes are provided in Fig. S1.

Inspired by platypus's predation process, we develop a bimodal deep learning framework to fuse the triboelectric and visuotactile signals simultaneously, as shown in Fig. 1f. At the input side, touchless perception carried by the triboelectric signal merges seamlessly with the multimodal tactile perception conveyed by visuotactile signal. Such fusion could suppress the interference generated during the touchless and tactile sensing process.

2.2. EM-Finger for touchless and tactile interaction

The EM-Finger has a compact structure, and its size is comparable to a human finger. And the photographs of the EM-Finger and its highly conductive LMPC pattern are shown in Fig. 2a and Fig. S2. The working principle of the triboelectric sensors is based on both contact electrification and electrostatic induction. A complete touchless and tactile perception process of the triboelectric sensor can be divided into multiple stages (Fig. 2b). At the initial stage (i), after several repeated contacts and separations, the PDMS dielectric layer and the external object (e.g., glass) generate equal but opposite charges due to the different electron affinities between two materials. In stage (ii), when the external object approaches the PDMS dielectric layer, the built-in electric field of the triboelectric sensor changes with decreasing distance, resulting in free electrons flowing from the ground to the electrodes and a current being generated in the circuit. As a result, a voltage signal across the resistor can be detected and recorded. At stage (iii), the external object and the PDMS dielectric layer come into contact, and at this time, the potential difference measured across the resistor would reach its maximum. When the external object separates from the dielectric layer, free electrons flow back from the electrode to the ground as the distance increases, generating a reverse voltage signal. Eventually, when the external object returns to its original position, the charges on both sides are rebalanced gradually. The charge transfer process for the triboelectric sensor with a negative charge external object is illustrated in Note S1. To visualize the potential distribution of the triboelectric sensor array and the external object during the working process, a finite element analysis with the COMSOL software is performed, as shown in Fig. 2c, (touchless sensing), Fig. 2g (tactile perception), and Fig. S3 (the external object rotates around the EM-Finger).

A measurement system is designed and utilized to investigate the triboelectric and visuotactile performance of the EM-Finger. The schematic diagrams are shown in Fig. S4 and Fig. S5, and a demonstration of the working process of the system is shown in Video S1. The EM-Finger is attached to a force sensor via a 3D-printed connector. And a $10 \times 10 \times 0.3$ cm aluminum (Al) plate is fixed on a linear motor which takes the Al plate for reciprocating motion. Meanwhile, the touchless sensing sensitivity of the triboelectric sensor array is also tested on the measurement system. The voltage signal output by the triboelectric sensor can be influenced by the movements of external objects (Fig. 2d). The voltage of the triboelectric sensor steadily increases as the positively charged Al plate approaches it. Conversely, when the Al plate moves away, an opposite voltage signal will be generated by the sensor. Apparently, the output voltage can be affected by the distance between the EM-Finger and the external object. As the distance increases from 1 to 20 cm, the voltage decreases exponentially from 55.5 mV to 1.1 mV (Fig. 2e). And the voltage signals recorded from the three triboelectric sensors (E1, E2, E3) will be changed with the angle (0°, 120°, 360°) between the external object and the EM-Finger (Fig. 2f), indicating that the touchless sensing of the EM-Finger is omnidirectional and can locate external objects in space (Fig. S6). Based on the polarity and amplitude of the voltage signals recorded from the triboelectric sensor array, the movement information of the external objects can be analyzed.

Supplementary material related to this article can be found online at doi:10.1016/j.nanoen.2023.108790.

Furtherly, the effect of the external objects with different materials on the output voltage of the triboelectric sensor is investigated. Different waveforms generated by the triboelectric sensor under the influence of five different materials are compared and analyzed (Fig. 2h). Since wood has the highest electropositivity among the five materials, the triboelectric sensor will have the largest output when the wood contacts it. While the fluorinated ethylene propylene (FEP) film with a high electronegativity approaches the EM-Finger, a waveform with the opposite direction can be generated. The experiment results indicate that the amplitude and polarity of the voltage signal generated by the triboelectric sensor are affected by the intrinsic property of the external object. In addition, the voltage of the triboelectric sensor increases from 0.3 V to about 1.2 V as the contact pressure increases from 2 N to 10 N (Fig. 2i), while the voltage generated during the contact process is significantly larger than that generated in the non-contact process (Fig. S7). Under the same contact condition with a pressure of 4 N, the triboelectric sensor works for 10,000 cycles in 3.5 h. As shown in Fig. 2j, the comparison of the voltage signals before and after the working process indicates that the triboelectric sensor has good durability.

Notably, in contact situation, the voltage signal of the triboelectric sensor is affected by both the polarity of the object material and the contact pressure, resulting in difficulty for decoupling the pressure and material information. To address this issue, the visuotactile sensing approach is utilized to record the different pressures in real time. And several experiments are conducted to demonstrate that the EM-Finger can be used to identify the contact pressure and surface texture of external objects. Fig. 2k and l show the schematic diagram of the elastomer and the variation of the internal markers in their locations and areas when the EM-Finger is subjected to different forces (normal and shear forces). The strain and stress distribution of the elastomer when in contact with an external object is also analyzed using finite element analysis (Fig. S8). And a micro camera with a sampling rate of 30 frames per second and a resolution of 640×480 pixels is utilized to record the images of the elastomer and markers throughout the whole working process. When the external object contacts with the EM-Figure in different positions, the images of the elastomer and markers are shown in Fig. S9. The results demonstrate that the EM-Finger can perceive the contact position on the entire 3D surface. Furthermore, under different pressures, the markers in the fingertip show differences in their areas and locations (Fig. 2m and Fig. S10). By analyzing these changes via advanced image pre-processing method, multidirectional forces can be detected and identified by the system (Table S1 and Video S2). In addition, the excellent durability of the visuotactile sensor for force sensing is shown in Fig. S11. When an external force is applied on the EM-Figure by a patterned pen, the captured tactile image can provide a clear visualization of the pen's textural information (Fig. 2n). And more texture perception experiments for other external objects are shown in Fig. S12. Such results intuitively demonstrate that the EM-Finger can be used for omnidirectional touchless sensing and multimodal tactile perception.

Supplementary material related to this article can be found online at doi:10.1016/j.nanoen.2023.108790.

2.3. Deep-learning-enabled material identification system

In order to effectively interact with the real world, the EM-Finger should possess similar abilities to human skin in inferring the material types of contacted objects. However, identifying the material type of an

object is a great challenge for human skin, especially for objects with similar surfaces (Fig. 3a). It is worth noting that the triboelectric sensor has made significant progress in material recognition applications[41, 42], but the output signal is still vulnerable environmental factors, such as varying contact forces. This interference hinders the direct application of triboelectric sensors in practical sensing tasks. Nonetheless, by combining the proposed EM-Finger with a deep learning-assisted material identification system, we can recognize the material types of common objects in real-time, exhibiting outstanding capabilities beyond human skin perception. We design an experimental system comprising the EM-Finger and a linear motor. We select 18 types of materials (Fig. 3b), including acrylic, glass, and resin, etc. With the aid of the acquisition module, we are able to precisely record the triboelectric and visuotactile signals. Additionally, during the experiment, we extract pressure information from the visuotactile images.

We collect the triboelectric and pressure signals generated while the EM-Finger contacts with test materials under four predetermined pressures (2 N, 4 N, 6 N, 8 N) (Fig. 3c). To enhance the accuracy of material identification and extract more hidden features from the signals, we introduce deep learning architecture. The flowchart for material identification is shown in Fig. 3d. First, after preprocessing the data collected from known materials, we divide the data into training data and test data at a ratio of 7:3 and then combine it with a long short-term memory full convolutional network (LSTM-FCN) model, and iterate continuously. As the amount of training data increases, the deep learning model gradually approaches the actual situation.

As shown in Fig. 3e, we have achieved high accuracy in material perception for all 18 tested materials using the triboelectric and pressure signals. We also compare the recognition learning curves with and without the pressure signal (Fig. 3f), and the results show that the material recognition accuracy increased from 67.4 % to 94.4 % after fusing the pressure signal (Fig. S13). The interface of the tactile sensing system for material recognition can display the triboelectric and pressure signals, and the identification result can be displayed on the computer in real-time (Fig. 3g and Video S3).

Supplementary material related to this article can be found online at doi:10.1016/j.nanoen.2023.108790.

2.4. HRI and feedback platform based on EM-finger

To further explore an integrated interaction method between robots and humans, we propose a flexible interface with the EM-Finger (Fig. 4a). Combined with the touchless and tactile sensing capabilities, we demonstrate that humans could touchless control the robotic arm in 3D space with an FEP film. When manipulating objects, the EM-Finger could provide multimodal tactile perception (Video S4 and S5). Here, we mount the EM-Finger on an AUBO i5 robotic arm and record bimodal information during the entire interaction. The EM-Finger's three side-electrodes (E1, E2, E3) can encode three-channel triboelectric signals into the interaction commands between the operator and the robotic arm. At the same time, the triboelectric signal generated by the E4 electrode and the pressure extracted from the visuotactile sensor will be used for object material identification during the contact process of the EM-Finger with the object. The detailed robotic arm interaction strategy can be found in Fig. S14 and Table S2.

Supplementary material related to this article can be found online at doi:10.1016/j.nanoen.2023.108790.

The bimodal signals and the recognition results (force, material, and texture) are displayed in real-time on a computer screen for easy visibility to the operator. Fig. 4b shows the effect of the obstacle occlusion between the human and the EM-Finger on the signal. In this experiment, a 50 × 50 × 0.5 cm acrylic plate is placed between the operator and the EM-Finger, where the distance between the operator and the EM-Finger is about 10 cm. The obstacle causes a significant reduction in the touchless signal. However, the EM-Finger still clearly detects the interaction command, indicating that the electrostatic induction exhibits strong resistance to obstacles (Video S6).

Supplementary material related to this article can be found online at doi:10.1016/j.nanoen.2023.108790.

Fig. 4c illustrates the peak values of the touchless signal generated by channel E1, E2, and E3 during 50 repetitions of sliding the human finger close to the E1 electrode. The signal obtained from the E1 electrode consistently exhibits higher amplitudes than the other two channels, indicating that EM-Finger can sense spatial motion from different directions. In addition, the signals from the three channels are encoded to six corresponding motion commands, enabling the control of the robot arm in 3D space (Fig. 4d). The human interactively operates the robotic arm to accurately identify the object and move it to the assigned working area. The whole interaction process can be divided into five steps (Fig. 4e).

In step (i), the operator's finger slides downward in the E1 direction without contact, and the three channels generate touchless signals while the pressure signal remains zero (Fig. 4f). In step (ii), according to the motion command recognized by the computer, the robotic arm is controlled to move horizontally in the direction of E1, and the operator slides again until the arm is adjusted to a position vertically above the measured object. In step (iii), the robotic arm moves downward to identify the object, the E4 electrode generates a larger triboelectric signal, and the pressure signal increases sharply for a short time. As the robotic arm moves upwards, the EM-Finger separates from the object, and a lower peak appears in the triboelectric signal, while the pressure signal becomes zero, enabling correct material identification based on the bimodal information. In step (iv), the arm moves downward and contacts the correctly identified object, and the triboelectric signal and multidirectional force signal (normal and shear forces) increase suddenly at the moment of contact (Fig. S15). After that, the arm keeps contact with the object and pushes it to the assigned working area, while the triboelectric signal is zero, and the multidirectional force signal changes continuously. In step (v), the robotic arm moves upward, the EM-Finger is separated from the object, and the triboelectric signal generates a lower peak while the pressure signal returns to zero. Finally, we successfully touchless control the robotic arm equipped with EM-Finger to identify and manipulate objects. The experimental results demonstrate an interaction paradigm between humans and robots through EM-Finger, which is constructed with simplicity and efficiency.

2.5. Underwater remote control and exploration

The complexity of the underwater environment has long been the barrier that prevents the further application of tactile sensing [43,44]. As depicted in Fig. 5a, the platypus can perceive the weak bioelectric signal generated by prey through its abundant electroreceptors. This ability allows the platypus to determine the location of surrounding preys. Taking full advantage of EM-Finger's compact structure and flexible electrosensory capabilities, a remote control and exploration system for underwater applications are constructed using a controllable electric field source (Fig. 5b). In this system, the spring-assisted triboelectric nanogenerator (S-TENG) generates an electrical signal from a mechanical source and can transmit through the water to control underwater unmanned robots for exploration activities. Refer to Note S2 for the specific working principle of S-TENG. By controlling an external triboelectric nanogenerator, different electrical signals can be propagated underwater [45], For example, setting larger peaks as "1" represents a stronger pressing force, while setting smaller peaks as "0" represents a lighter pressing force. Therefore, we can use mechanically-driven S-TENG to generate artificial underwater electrical fields that mimic the bioelectric fields and achieve remote control of underwater robots through the water as the medium. To test the performance of remote underwater control, the transmitting electrode in water is connected to the Al electrode of the S-TENG. In contrast, the other electrode of the S-TENG is grounded, allowing the S-TENG to operate in single-electrode mode, as shown in the experimental setup

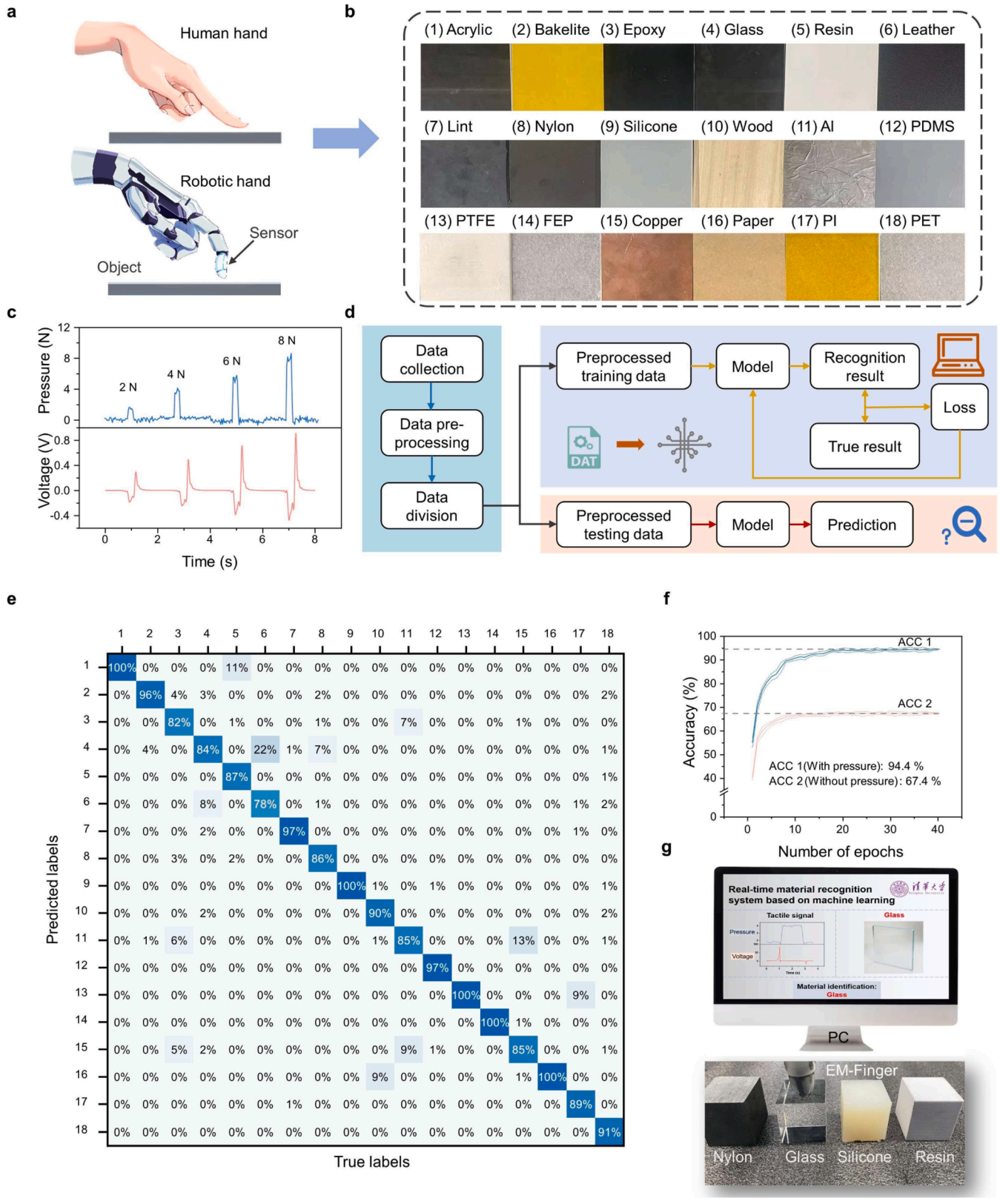

Fig. 3. Deep-learning-enabled tactile material identification system. (a) Schematic diagram of a robotic hand with integrated EM-Finger simulating human hand for material detection and (b) the corresponding 18 test materials. (c) Triboelectric signal and pressure signal when it detected materials in different pressure. (d) Flow diagram of machine learning for material identification. (e) The corresponding confusion map for 18 materials. (f) The prediction accuracy of material types under different data inputs, with or without pressure information. (g) Real-time display of the perception results for glass by using the constructed material perception system.

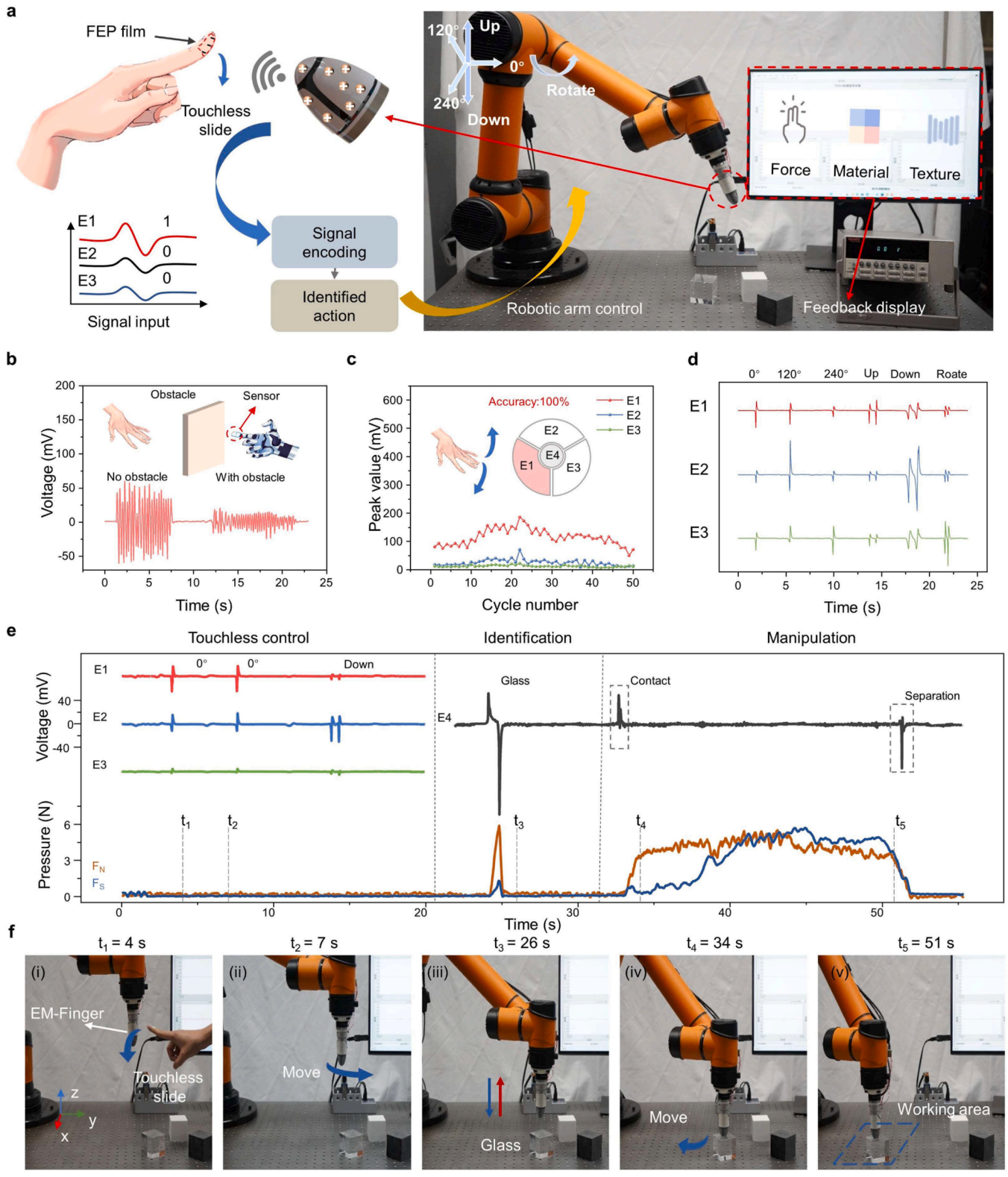

Fig. 4. Demonstration of the non-contact interaction and feedback system by the smart finger. (a) Schematic diagram of the non-contact interaction movement experiment with the EM-Finger through the FEP film at the tip of the human finger. (b) Influence of obstacle between the human hand and sensor on the signal. (c) Sliding on the side close to the E3 electrode, the signal output amplitude of each electrode of the EM-Finger is under 50 times sliding. (d) Interaction sensing data was collected by the three-channel electrodes from six motions. (e) Signal curves and (f) demonstration photograph of a robotic arm equipped with the EM-Finger interactively controlling, detecting, and moving a glass cube object.

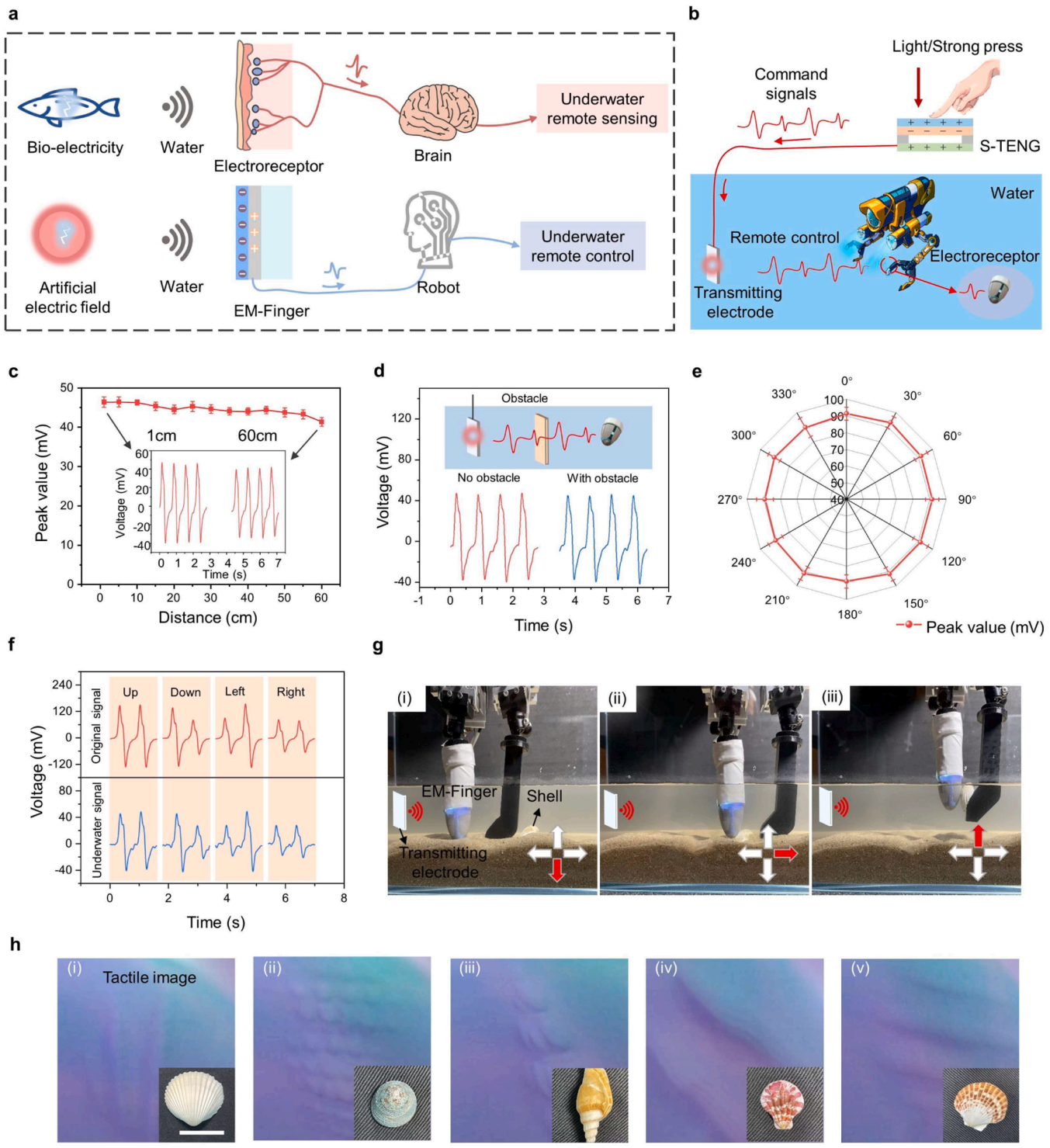

Fig. 5. Demonstration of the underwater remote interaction and exploration. (a) A schematic diagram describing the mechanism of artificial receptors that mimic the sensory system of the platypus for underwater remote control. In an underwater experiment, signal generated by an artificial electric field used to mimic bioelectricity are transmitted in the water. (b) Diagram of the button-type TENG remote control unmanned underwater probe with robotic gripper. (c) Variation of the peak values on the receiving voltage signal with the distance between the transmitting electrodes and EM-Finger. (d) Influence of an obstacle on the voltage signal. (e) Directional pattern evaluation of the EM-Finger in water. (f) Comparison between the original command signal and received signal in water for motion control. (g) The schematic diagram of underwater wireless remote robotic gripper control and object recognition. (h) Photographs of various types of shells and their corresponding tactile images (scale bar: 2 cm).

schematic in Fig. S16. For the specific working principle of the underwater remote control, see Note S3.

Fig. 5c shows the influence of different distances between the transmitting electrode and the EM-Finger on underwater signal propagation. The peak value of the received signal in the water tank decreases as the distance between the transmitting electrode and the EM-Finger increases. When the distance between them increases to 60 cm, the signal's peak value hardly decreases. Additionally, the ability

to keep signal robustness is also critical for communication requirements in complex underwater. As shown in Fig. 5d, even with obstacles placed in the water tank, the received signal waveform remains the same as the original signal, indicating the robustness of the polarized electric field against obstacles. Fig. 5e shows the influence of different angles (in the horizontal direction) of the transmitting electrode on the underwater signal. With the change of signal incident angle, the voltage signal remains stable, indicating that the underwater electrical reception ability is omnidirectional. Fig. 5f compares the signal from the original S-TENG with the signal in water, showing significant attenuation but maintaining a consistent waveform with the original signal. The voltage signal generated by mechanical pressing of the S-TENG can be encoded as control commands, enabling underwater remote control for up, down, left, and right movements.

Based on these results, we install the EM-Finger on the end of the robotic gripper (Fig. S17) to achieve remote underwater interaction and high-resolution tactile perception, mimicking the feeding behavior of platypus using its mouth to prey in mud, thus determining relevant environmental information for underwater tasks. By controlling the movement of the robotic gripper in water and utilizing different tactile perception information, successful object recognition and manipulation are achieved underwater (Fig. 5g). It should be noted that EM-Finger provides high-resolution tactile information even underwater. Fig. 5h shows the tactile image while grasping bivalves, which can recognize the typical features of shells based on the high-resolution visuotactile image. These features are the main characteristics of various bivalves (Fig. S18 and Video S7). This process mimics the entire process of a platypus feeding underwater using its electroreceptors and mechanoreceptors.

Supplementary material related to this article can be found online at doi:10.1016/j.nanoen.2023.108790.

3. Conclusion

The rich tactile perception and interactive capabilities of robots are of great significance in practical applications. In this study, inspired by the platypus beak sense, the electro-mechanosensory finger is designed, which is composed of a triboelectric sensor array and a finger-shaped visuotactile sensor. To improve the integration of EM-Finger, an LMPC layer simultaneously serves as the electrode layer of the triboelectric sensor array and the reflector of the visuotactile sensor. Based on contact electrification and electrostatic induction effects, the triboelectric sensor array can encode both touchless and tactile interactions into voltage signals in the air, and detect the electrical stimuli underwater for amphibious wireless communication. Meanwhile, the high-resolution visuotactile sensor can provide multimodal tactile information, including contact pressure and surface texture. With the deep learning architecture fusing the triboelectric and visuotactile signals, the identification accuracy of material under varying forces is significantly improved to 94.4 %. The omnidirectional touchless sensing and multimodal tactile perception of the EM-Finger make it possible for robots to carry out remote control and object recognition in the air. In addition, the integrated system can perform touchless HRI and high-resolution tactile sensing in complex underwater environments, even in the presence of obstacles.

Compared with other existing approaches for multisensory sensing, the bimodal EM-Finger exhibits advantages in high integration and portability (refer to Table S3 and Table S4). Although more computing resources are consumed when processing visuotactile data, high-resolution tactile perception is still essential when performing some complex manipulation and identification tasks. Going forward, more challenging and practical applications can be realized by building interfaces between EM-Finger and robots. For example, it can help robots carry out exploration and manipulation in situations where vision is obstructed. At the same time, the highly integrated and finger-shaped structural design may enhance the humanoid robot's perception of the external environment. We envision that the fusion of EM-Finger and intelligent motion control of robots will further facilitate the development of the enhanced HRI application.

4. Methods

4.1. Fabrication process of soft transparent fingertip

A 3D-printed mold with a semi-elliptical groove was prepared for fabricating the silicone-based transparent elastomer. The elastomer was fabricated with the mixture of PDMS (Sylgard 184, Dow Corning, USA, weight ratio = 10:1) and transparent silicone (Shinbon, China) at a ratio of 2:1. The mixture was first degassed in a vacuum chamber for 10 min to avoid air bubbles, and then cured at 60 °C for 3 h. After this, a 3D-printed mask with three markers was placed on the cured elastomer, then three black markers (silicone doped with black pigment) were added in turn. After the second curing, the unit with the markers is complete and ready for applying a liquid metal-based conductive and reflective layer.

4.2. Fabrication process of the triboelectric sensor array with liquid metal

We added 1.5 g of EGaIn (Ga: In = 4:1, Zhongchuang Alloy, China) and 1 g 3 wt % PVP (Aladdin, China) decanol (98 %, MACKLIN, China) solution to a 5 mL EP tube and sonicated (Lichen ultrasonic cell disruptor, China) the tube in an ice-water bath for 5 min (amplitude of 20 %, 5 s on and 5 s off in each cycle) to fabricate the liquid metal-polymer suspension microparticles. We added the prepared composite into the airbrush (0.5 mm caliber) and sprayed it on the transparent fingertip with a patterned mask. Then, we placed the fingertip at 50 °C for 1 h to evaporate the solvent and remove the mask. To cover the area between the patterned liquid metal, non-conductive silver-grey silicone pigments were sprayed onto the cured fingertip. The PDMS was drop-casted onto the patterned liquid metal and then cured at room temperature for four hours to finish the encapsulation.

4.3. Assembly and connection of EM-Finger

Components for connection or assembly are 3D printed with polylactic acid (PLA) filament. Noteworthy, considering the different stiffness of the flexible elastomer and the 3D printed part, we use silicone adhesive (Sil-Proxy, Smooth-On, USA) to connect them.

4.4. Characterization of the triboelectric sensor for touchless/tactile sensing

An electrometer measured the signal outputs in the triboelectric sensor's characterization (Keithley, 6514, USA). The multi-channel signals were conducted by a synchronous data acquisition module (National Instruments, USB-6356, USA) and displayed by the LabVIEW software. The basic movement platform used a linear motor (LinMot, E1100, Switzerland) to simulate the manipulator for contact and separation (initial distance, 40 cm). The pressure during contact is measured by a high-precision pressure sensor (ATI Industrial Automation, Mini40, USA) and recorded by the accompanying software.

4.5. Finite element analysis

To verify the theoretical accuracy of our design, we conducted multiphysics simulations, which encompassed both motion and electric fields. The simulations were performed using the COMSOL Multiphysics software, specifically utilizing its electric field module and structural mechanics module. To simulate the sensor's deformation, we constructed a 3D model of the sensor within COMSOL and employed the structural mechanic's module to analyze how the sensor deformed under various external forces. Regarding the potential distribution of the

sensor, we assumed that the sensor was fully charged, possessing the maximum charge that could be accumulated on its effective detection surface. In our 3D simulations, we set the surrounding free space to a distance of 15 m, ensuring that the free space was practically infinite compared to the sensor.

4.6. Deep learning enabled by LSTM-FCN

The LSTM-FCN model is often used to process spatial features in time-series data. It combines the capabilities of LSTM, which can capture long-term dependencies, and FCN, which can efficiently extract spatial features from data. Here we built the LSTM-FCN model based on the Pytorch library. After continuous validation and iteration on the training set data, the pre-trained model is validated on the test data. In addition, we conducted further experiments under consistent hyperparameters, evaluating the learning capability of the LSTM-FCN model on both single triboelectric and multimodal signals.

CRediT authorship contribution statement

S. Mu., W. Lee., C. Wu., and W. Ding. conceived the idea, designed the experiment, and guided the project. S. Mu., S. Li., H. Zhao., and Z. Wang. fabricated the triboelectric sensor array, characterized, and tested the EM-Finger. X. Xiao., X. Xiao., and H. Tang. performed the simulation. Z. Lin., Z. Song., Q. Xu., and D. Wang. designed mechanical structure and acquisition circuit. S. Mu., C. Wu., and W. Ding. analyzed the experimental data, drew the figures, and prepared the manuscript. All authors reviewed and commented on the manuscript.

Declaration of Competing Interest

The authors declare that they have no known competing financial interests or personal relationships that could have appeared to influence the work reported in this paper.

Data Availability

Data will be made available on request.

Acknowledgments

The authors are grateful for the joint support from the National Natural Science Foundation of China (62104125 and 62311530102), the Tsinghua Shenzhen International Graduate School-Shenzhen Pengrui Young Faculty Program of Shenzhen Pengrui Foundation (Grant No. SZPR2023005), the Shenzhen Science and Technology Program JCYJ20220530143013030, Guangdong Innovative and Entrepreneurial Research Team Program 2021ZT09L197.

Appendix A. Supporting information

Supplementary data associated with this article can be found in the online version at doi:10.1016/j.nanoen.2023.108790.

References

[1] Y. Liu, C. Yiu, Z. Song, Y. Huang, K. Yao, T. Wong, J. Zhou, L. Zhao, X. Huang, S. K. Nejad, M. Wu, D. Li, J. He, X. Guo, J. Yu, X. Feng, Z. Xie, X. Yu, Electronic skin as wireless human-machine interfaces for robotic VR, Sci. Adv. 8 (2022) eabl6700, https://doi.org/10.1126/sciadv.abl6700.

[2] S. Mintchev, M. Salerno, A. Cherpillod, S. Scaduto, J. Paik, A portable three-degrees-of-freedom force feedback origami robot for human–robot interactions, Nat. Mach. Intell. 1 (2019) 584–593, https://doi.org/10.1038/s42256-019-0125-1.

[3] B. Hou, L. Yi, C. Li, H. Zhao, R. Zhang, B. Zhou, X. Liu, An interactive mouthguard based on mechanoluminescence-powered optical fibre sensors for bite-controlled device operation, Nat. Electron. 5 (2022) 682–693, https://doi.org/10.1038/s41928-022-00841-8.

[4] L. Li, S. Wang, Y. Zhang, S. Song, C. Wang, S. Tan, W. Zhao, G. Wang, W. Sun, F. Yang, J. Liu, B. Chen, H. Xu, P. Nguyen, M. Kovac, L. Wen, Aerial-aquatic robots capable of crossing the air-water boundary and hitchhiking on surfaces, Sci. Robot. 7 (2022) eabm6695, https://doi.org/10.1126/scirobotics.abm6695.

[5] X. Hui, Z. Li, L. Tang, J. Sun, X. Hou, J. Chen, Y. Peng, Z. Wu, H. Guo, A self-powered, highly embedded and sensitive tribo-label-sensor for the fast and stable label printer, Nano-Micro Lett. 15 (2023), 27, https://doi.org/10.1007/s40820-022-00999-y.

[6] K.K. Kim, M. Kim, K. Pyun, J. Kim, J. Min, S. Koh, S.E. Root, J. Kim, B.-N. T. Nguyen, Y. Nishio, S. Han, J. Choi, C.-Y. Kim, J.B.-H. Tok, S. Jo, S.H. Ko, Z. Bao, A substrate-less nanomesh receptor with meta-learning for rapid hand task recognition, Nat. Electron. 6 (2023) 64–75, https://doi.org/10.1038/s41928-022-00888-7.

[7] X. Zhang, L. Lu, W. Wang, N. Zhao, P. He, J. Liu, B. Yang, Flexible pressure sensors with combined spraying and self-diffusion of carbon nanotubes, ACS Appl. Mater. Interfaces 14 (2022) 38409–38420, https://doi.org/10.1021/acsami.2c12240.

[8] B.W. An, S. Heo, S. Ji, F. Bien, J.-U. Park, Transparent and flexible fingerprint sensor array with multiplexed detection of tactile pressure and skin temperature, Nat. Commun. 9 (2018) 2458, https://doi.org/ 10.1038/s41467-018-04906-1.

[9] Q. Su, Q. Zou, Y. Li, Y. Chen, S.-Y. Teng, J.T. Kelleher, R. Nith, P. Cheng, N. Li, W. Liu, S. Dai, Y. Liu, A. Mazursky, J. Xu, L. Jin, P. Lopes, S. Wang, A stretchable and strain-unperturbed pressure sensor for motion interference–free tactile monitoring on skins, Sci. Adv. 7 (2021) eabi4563, https://doi.org/10.1126/sciadv.abi4563.

[10] Y. Yan, Z. Hu, Z. Yang, W. Yuan, C. Song, J. Pan, Y. Shen, Soft magnetic skin for super-resolution tactile sensing with force self-decoupling, Sci. Robot 6 (2021) eabc8801, https://doi.org/ 10.1126/scirobotics.abc8801.

[11] B. Fang, Z. Xia, F. Sun, Y. Yang, H. Liu, C. Fang, Soft magnetic fingertip with particle-jamming structure for tactile perception and grasping, IEEE Trans. Ind. Electron 70 (2023) 6027–6035, https://doi.org/10.1109/TIE.2022.3201305.

[12] J. Zhou, Q. Shao, C. Tang, F. Qiao, T. Lu, X. Li, X. Liu, H. Zhao, Conformable and compact multiaxis tactile sensor for human and robotic grasping via anisotropic waveguides, Adv. Mater. Technol. 7 (2022) 2200595, https://doi.org/10.1002/admt.202200595.

[13] C. Jiang, Z. Zhang, J. Pan, Y. Wang, L. Zhang, L. Tong, Finger-skin-inspired flexible optical sensor for force sensing and slip detection in robotic grasping, Adv. Mater. Technol. 6 (2021) 2100285, https://doi.org/10.1002/admt.202100285.

[14] H. Sun, K.J. Kuchenbecker, G. Martius, A soft thumb-sized vision-based sensor with accurate all-round force perception, Nat. Mach. Intell. 4 (2022) 135–145, https://doi.org/10.1038/s42256-021-00439-3.

[15] S.Q. Liu, E.H. Adelson, GelSight Fin Ray: incorporating tactile sensing into a soft compliant robotic gripper, Proc. IEEE Int. Conf. Soft Robot. Edinb. U. Kingd. (2022) 925–931, https://doi.org/10.1109/ROBOSOFT54090.2022.9762175.

[16] C. Trueeb, C. Sferrazza, R. D'Andrea, Towards vision-based robotic skins: a data-driven, multi-camera tactile sensor, Proc. IEEE Int. Conf. Soft Robot. N. Haven CT U S A (2020) 333–338, https://doi.org/10.1109/RoboSoft48309.2020.9116060.

[17] W.K. Do, M. Kennedy, DenseTact: optical tactile sensor for dense shape reconstruction, Proc. IEEE Int. Conf. Robot. Autom., Phila., U S A (2022) 6188–6194, https://doi.org/10.1109/ICRA46639.2022.9811966.

[18] B. Romero, F. Veiga, E. Adelson, Soft, Round, High Resolution Tactile Fingertip Sensors for Dexterous Robotic Manipulation, in: Proceedings of the IEEE Int. Conf. Robot. Autom., Paris, France, (2020) 4796–4802, https://doi.org/ 10.1109/ICRA40945.2020.9196909.

[19] Z.H. Guo, H.L. Wang, J. Shao, Y. Shao, L. Jia, L. Li, X. Pu, Z.L. Wang, Bioinspired soft electroreceptors for artificial precontact somatosensation, Sci. Adv. 8 (2022) eabo5201, https://doi.org/ 10.1126/sciadv.abo5201.

[20] G.S. Cañón Bermúdez, D.D. Karnaushenko, D. Karnaushenko, A. Lebanov, L. Bischoff, M. Kaltenbrunner, J. Fassbender, O.G. Schmidt, D. Makarov, Magnetosensitive e-skins with directional perception for augmented reality, Sci. Adv. 4 (2018) eaao2623, https://doi.org/10.1126/sciadv.aao2623.

[21] S. Zhu, Y. Li, H. Yelemulati, X. Deng, Y. Li, J. Wang, X. Li, G. Li, P. Gkoupidenis, Y. Tai, An artificial remote tactile device with 3D depth-of-field sensation, Sci. Adv. 8 (2022) eabo5314, https://doi.org/10.1126/sciadv.abo5314.

[22] S. Geng, S. Fan, H. Li, Y. Qi, C. An, E. Wu, J. Su, J. Liu, An artificial neuromuscular system for bimodal human–machine interaction, Adv. Funct. Mater. (2023) 2302345, https://doi.org/10.1002/adfm.202302345.

[23] C. Zhang, K. Dai, D. Liu, F. Yi, X. Wang, L. Zhu, Z. You, Ultralow quiescent power-consumption wake-up technology based on the bionic triboelectric nanogenerator, Adv. Sci. 7 (2020) 2000254, https://doi.org/10.1002/advs.202000254.

[24] R. Liu, Y. Lai, S. Li, F. Wu, J. Shao, D. Liu, X. Dong, J. Wang, Z.L. Wang, Ultrathin, transparent, and robust self-healing electronic skins for tactile and non-contact sensing, Nano Energy 95 (2022), 107056, https://doi.org/10.1016/j.nanoen.2022.107056.

[25] J. Ge, X. Wang, M. Drack, O. Volkov, M. Liang, G. Bermudez, R. Illing, C. Wang, S. Zhou, J. Fassbender, M. Kaltenbrunner, D. Makarov, A bimodal soft electronic skin for tactile and touchless interaction in real time, Nat. Commun. 10 (2019) 4405, https://doi.org/10.1038/s41467-019-12303-5.

[26] Q. Zhou, B. Ji, B. Hu, S. Li, Y. Xu, Y. Gao, W. Wen, J. Zhou, B. Zhou, Tilted magnetic micropillars enabled dual-mode sensor for tactile/touchless perceptions, Nano Energy 78 (2020), 105382, https://doi.org/10.1016/j.nanoen.2020.105382.

[27] W. Liu, Y. Duo, J. Liu, F. Yuan, L. Li, L. Li, G. Wang, B. Chen, S. Wang, H. Yang, Y. Liu, Y. Mo, Y. Wang, B. Fang, F. Sun, X. Ding, C. Zhang, L. Wen, Touchless interactive teaching of soft robots through flexible bimodal sensory interfaces, Nat. Commun. 13 (2022) 5030, https://doi.org/10.1038/s41467-022-32702-5.

[28] A. SaLoutos, E. Stanger-Jones, S. Kim, Fast reflexive grasping with a proprioceptive teleoperation platform, in: Proceedings of the IEEE Int. Conf. Intell. Robot. Syst., Kyoto, Japan, (2022) 6213–6220, https://doi.org/10.1109/IROS47612.2022.9981383.

[29] X. Ye, B. Shi, M. Li, Q. Fan, X. Qi, X. Liu, S. Zhao, L. Jiang, X. Zhang, K. Fu, L. Qu, M. Tian, All-textile sensors for boxing punch force and velocity detection, Nano Energy 97 (2022), 107114, https://doi.org/10.1016/j.nanoen.2022.107114.
[30] H.L. Wang, T. Chen, B. Zhang, G. Wang, X. Yang, K. Wu, Y. Wang, A dual-responsive artificial skin for tactile and touchless interfaces, Small 19 (2023) 2206830, https://doi.org/10.1002/smll.202206830.
[31] H. Guo, Y.J. Tan, G. Chen, Z. Wang, G.J. Susanto, H.H. See, Z. Yang, Z.W. Lim, L. Yang, B.C.K. Tee, Artificially innervated self-healing foams as synthetic piezo-impedance sensor skins, Nat. Commun. 11 (2020) 5747, https://doi.org/10.1038/s41467-020-19531-0.
[32] M. Liu, Y. Zhang, J. Wang, N. Qin, H. Yang, K. Sun, J. Hao, L. Shu, J. Liu, Q. Chen, P. Zhang, T.H. Tao, A star-nose-like tactile-olfactory bionic sensing array for robust object recognition in non-visual environments, Nat. Commun. 13 (2022), 79, https://doi.org/10.1038/s41467-021-27672-z.
[33] G. Lee, J. Son, D. Kim, H.J. Ko, S.G. Lee, K. Cho, Crocodile-skin-inspired omnidirectionally stretchable pressure sensor, Small 18 (2022) 2205643, https://doi.org/10.1002/smll.202205643.
[34] S. Wang, P. Xu, X. Wang, J. Zheng, X. Liu, J. Liu, T. Chen, H. Wang, G. Xie, J. Tao, M. Xu, Underwater bionic whisker sensor based on triboelectric nanogenerator for passive vortex perception, Nano Energy 97 (2022), 107210, https://doi.org/10.1016/j.nanoen.2022.107210.
[35] R. Kempster, S. Collin, Electrosensory pore distribution and feeding in the megamouth shark Megachasma pelagios (Lamniformes: Megachasmidae), Aquat. Biol. 11 (2011) 225–228, https://doi.org/10.3354/ab00311.
[36] N.W. Bellono, D.B. Leitch, D. Julius, Molecular basis of ancestral vertebrate electroreception, Nature 543 (2017) 391–396, https://doi.org/10.1038/nature21401.
[37] H. Scheich, G. Langner, C. Tidemann, R.B. Coles, A. Guppy, Electroreception and electrolocation in platypus, Nature 319 (1986) 401–402, https://doi.org/10.1038/319401a0.
[38] J.D. Pettigrew, P.R. Manger, S.L. Fine, The sensory world of the platypus, Philos. Trans. R. Soc. Lond. B Biol. Sci. 353 (1998) 1199–1210, https://doi.org/10.1098/rstb.1998.0276.
[39] J.D. Pettigrew, Electroreception in monotremes, J. Exp. Biol. 202 (1999) 1447–1454, https://doi.org/10.1242/jeb.202.10.1447.
[40] M.K. Johnson, F. Cole, A. Raj, E.H. Adelson, Microgeometry capture using an elastomeric sensor, ACM Trans. Graph 30 (2011) 1–8, https://doi.org/10.1145/1964921.1964941.
[41] G.G. Lee, J.H. Son, S. Lee, S.W. Kim, D. Kim, N.N. Nguyen, S.G. Lee, K. Cho, Fingerpad-inspired multimodal electronic skin for material discrimination and texture recognition, Adv. Sci. 8 (2021) 2002606, https://doi.org/10.1002/advs.202002606.
[42] Z. Song, J. Yin, Z. Wang, C. Lu, Z. Yang, Z. Zhao, Z. Lin, J. Wang, C. Wu, J. Cheng, Y. Dai, Y. Zi, S.-L. Huang, X. Chen, J. Song, G. Li, W. Ding, A flexible triboelectric tactile sensor for simultaneous material and texture recognition, Nano Energy 93 (2022), 106798, https://doi.org/10.1016/j.nanoen.2021.106798.
[43] Y. Cheng, C. Guo, S. Li, K. Deng, J. Tang, Q. Luo, S. Zhang, Y. Chang, T. Pan, Aquatic skin enabled by multi-modality iontronic sensing, Adv. Funct. Mater. 32 (2022) 2205947, https://doi.org/ 10.1002/adfm.202205947.
[44] S. Li, X. Yin, C. Xia, L. Ye, X. Wang, B. Liang, TaTa: A universal jamming gripper with high-quality tactile perception and its application to underwater manipulation, in IEEE Int. Conf. Robot. Autom., Philadelphia, PA, USA, (2022) 6151–6157, https://doi.org/10.1109/ICRA46639.2022.9811806.
[45] H. Zhao, M. Xu, M. Shu, J. An, W. Ding, X. Liu, S. Wang, C. Zhao, H. Yu, H. Wang, C. Wang, X. Fu, X. Pan, G. Xie, Z.L. Wang, Underwater wireless communication via TENG-generated Maxwell's displacement current, Nat. Commun. 13 (2022) 3325, https://doi.org/10.1038/s41467-022-31042-8.

Shilong Mu received his B.S. degree in Electronic Information Engineering from China University of Mining and Technology in 2022. He is currently pursuing his M.S. degree in Data Science and Information Technology at Smart Sensing and Robotics (SSR) group at Tsinghua University. His research interests focus on tactile sensing and feedback reconstruction, soft robotics, and electronic skin.

Shoujie Li received the B.Eng. degree in electronic information engineering from the College of Oceanography and Space Informatics, China University of Petroleum, Tsingtao, China, in 2020. He is currently pursuing toward Ph.D. degree in Tsinghua-Berkeley Shenzhen Institute, Shenzhen International Graduate School, Tsinghua University, Shenzhen, China. His research interests include tactile perception, grasping, and machine learning.

Hongfa Zhao received his M.S. degree in Marine Engineering from Dalian Maritime University in 2021. He is currently pursuing his Ph.D. degree in Data Science and Information Technology at Tsinghua-Berkeley Shenzhen Institute, Tsinghua University. His research interests mainly focus on design and theoretical analysis for triboelectric nanogenerators.

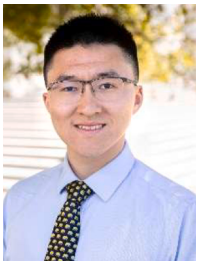

Zihan Wang received his dual BEng. degrees (1st class Hons.) from Xidian University and Heriot-Watt University in 2019. He is currently pursuing his Ph.D. degree in Data Science and Information Technology at Smart Sensing and Robotics (SSR) group, Tsinghua-Berkely Shenzhen Institute, Tsinghua University. His research interests focus on intelligent sensory systems with their applications in soft robots and human-machine interfaces.

Xiao Xiao's current research interest is in Zn-based flexible batteries, bioelectronic devices, and ferromagnetic soft robots. Graduated from School of Material Science and Engineering of Beihang university, he is now pursuing his Doctor degree in New energy material group at Tsinghua University.

Xiao Xiao is a graduate student in Department of Electrical and Computer Engineering at the National University of Singapore. His research focuses on the intersection of flexible batteries, energy harvesting/delivery, and sensing technologies to develop solutions for next-generation bioelectronics. He holds 1 licensed patent, published 1 book chapter and 80 journal articles, and in 40 of them, he is the first/co-first/corresponding author such as Science Advances, Nature Biomedical Engineering, Chemical Reviews, Advanced Materials, Advanced Science, Matter, The Innovation, ACS Nano, and Nano Letters. With an H-index of 30, his work has garnered 3000 + global citations.

Zenan Lin received his B.S. degree in Electrical Engineering and Automation from China University of Mining and Technology in 2021. He is currently pursuing his M.S. degree in Data Science and Information Technology at Smart Sensing and Robotics (SSR) group, Tsinghua University. His research interests include Tactile sensing, Power management system of TENG.

Ziwu Song is a Ph.D. student majoring in Data Science and Information Technology in Tsinghua-Berkeley Shenzhen Institute, Tsinghua University. He received his B.S. degree (Hons.) in Mechanical Engineering from Nanjing University of Science and Technology in 2020. His research interests mainly focus on tactile sensing and soft robotics.

Huaze Tang received his B.S. degree in Communication Engineering from Southeast University in 2021. He is currently pursuing his M.S. degree in Data Science and Information Technology at Smart Sensing and Robotics (SSR) group at Tsinghua University. His research interests focus on signal processing with deep learning, reinforcement learning and soft robots.

Qinghao Xu received the B.S. degree and the M.S. degree from Nanjing University of Posts and Telecommunications in 2019 and 2022 respectively. He is currently a Ph.D. student in Data Science and Information Technology at Smart Sensing and Robotics (SSR) group, Tsinghua University. His current research interests mainly focus on neuromorphic computing and self-powered systems.

Dongkai Wang is now studying as a PhD candidate in Sensors and Microsystems Lab,Tsinghua-Berkeley Shenzhen Institute (TBSI), Tsinghua University.He received his bachelor degree from Harbin Institute of Technoloy,China, and his master degree from Johns Hopkins University, USA. His research interest lies in flexible electronics, 3D printing and soft robots.

Wang Wei Lee received his Ph.D. degree from the National University of Singapore (NUS) in 2016. He was a Postdoctoral Research Fellow with the Biomedical Institute for Global Health Research and Technology at NUS between 2016 and 2019. He joined Tencent Robotics X in April 2019 as an Advanced Research Scientist in charge of tactile sensor research. His interests include the development of robust tactile sensing technologies applicable to real-world applications. His work ranges from materials engineering, embedded systems, signal processing and communication to systems integration.

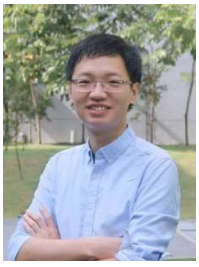

Changsheng WU is an assistant professor in the Department of Materials Science and Engineering (MSE) at the National University of Singapore (NUS). He is also a PI in the Institute for Health Innovation and Technology and the N.1 Institute for Health, NUS. He received his PhD in MSE from Georgia Tech and carried out postdoctoral research in the Querrey Simpson Institute for Bioelectronics at Northwestern University. His research focuses on developing wireless wearables and intelligent robots for energy harvesting, biosensing and therapeutic applications, leveraging bioelectronics, materials science, and advanced manufacturing to create solutions for sustainable living and environment.

Wenbo Ding received the BS and PhD degrees (Hons.) from Tsinghua University in 2011 and 2016, respectively. He worked as a postdoctoral research fellow at Georgia Tech under the supervision of Professor Z. L. Wang from 2016 to 2019. He is now an associate professor and PhD supervisor at Tsinghua-Berkeley Shenzhen Institute, Tsinghua Shenzhen International Graduate School, Tsinghua University, where he leads the Smart Sensing and Robotics (SSR) group. His research interests include mechanosensing, tactile sensing and robotics with the help of signal processing and machine learning. He has received many prestigious awards, including the Gold Medal of the 47th International Exhibition of Inventions Geneva and the IEEE Scott Helt Memorial Award.

View publication stats